AGU PUBLICATIONS

Geophysical Research Letters

RESEARCH LETTER
10.1002/2014GL061136

S. Karunatillake and J. J. Wray contributed equally.

Key Points:
- Sulfate subsurface abundance and hydration insight from gamma spectra
- H_2O:S molar ratio between 2.4 and 4.0 for 80% of the midlatitudes
- Regional association of H_2O with S in bulk soil at decimeter depth in the south

Supporting Information:
- Readme
- Figure S1 and Table S1

Correspondence to:
S. Karunatillake and J. J. Wray,
wk43@cornell.edu;
jwray@gatech.edu

Citation:
Karunatillake, S., J. J. Wray, O. Gasnault, S. M. McLennan, A. D. Rogers, S. W. Squyres, W. V. Boynton, J. R. Skok, L. Ojha, and N. Olsen (2014), Sulfates hydrating bulk soil in the Martian low and middle latitudes, *Geophys. Res. Lett.*, *41*, 7987–7996, doi:10.1002/2014GL061136.

Received 10 JUL 2014
Accepted 24 OCT 2014
Accepted article online 29 OCT 2014
Published online 22 NOV 2014

Sulfates hydrating bulk soil in the Martian low and middle latitudes

S. Karunatillake[1], J. J. Wray[2], O. Gasnault[3], S. M. McLennan[4], A. D. Rogers[4], S. W. Squyres[5], W. V. Boynton[6], J. R. Skok[1], L. Ojha[2], and N. Olsen[1]

[1]Department of Geology and Geophysics, Louisiana State University, Baton Rouge, Louisiana, USA, [2]Earth and Atmospheric Sciences, Georgia Institute of Technology, Atlanta, Georgia, USA, [3]IRAP, Université de Toulouse, UPS-OMP, Toulouse, France, [4]Department of Geosciences, State University of New York at Stony Brook, Stony Brook, New York, USA, [5]Department of Astronomy, Cornell University, Ithaca, New York, USA, [6]Lunar and Planetary Laboratory, University of Arizona, Tucson, Arizona, USA

Abstract The evidence for sulfate-bearing strata, across Late-Noachian to Amazonian eons, suggests a central role for sulfates in acidity and salinity of Martian paleofluids and the planet's habitability. However, details remain unclear owing to shallow sampling and the limited ability of visible/near-infrared spectroscopy to distinguish among some sulfates. Using chemical data from the Mars Odyssey gamma ray spectrometer, including the sulfur map of Mars, we confirm the possibility of hydrous sulfates acting as key hydrates throughout the southern midlatitudinal soil at decimeter depths. An H_2O:S molar ratio between 2.4 and 4.0 for 80% of the midlatitudes is also consistent with hydrous sulfate phases, including the many Fe sulfates hydrated in this range or mixtures of Ca and Mg sulfates. Nevertheless, hydrous Fe sulfates could explain our observations in a simpler manner relative to Ca/Mg mixtures. Furthermore, phyllosilicates, zeolites, amorphous phases, and H_2O(s) do not seem to be strong candidates to explain the H-S variations. Consequently, we speculate that sulfates, as the primary contributor of H_2O in bulk soil, may influence modern aqueous processes including warm-season slope lineae in the southern hemisphere.

1. Introduction

Some observations suggest that hydrous sulfates store most of the observed H_2O in the uppermost meter of the Martian subsurface soil at low latitudes [*Feldman et al.*, 2004; *Wang et al.*, 2013], but orbital visible/near-infrared spectrometers can identify them [e.g., *Wray et al.*, 2011; *Liu et al.*, 2012] only in the tens to hundreds of micron surficial layer. This surficial layer may not represent deeper subsurface soil, given compositional and mineralogical variations with depth observed in outcrop sections [e.g., *Roach et al.*, 2009], rock coatings [*Haskin et al.*, 2005], and soil trenches [e.g., *Arvidson et al.*, 2010]. Indeed, such variations are expected from a combination of recent aqueous activity, early diagenesis, and variations in the original depositional environment.

Landers and rovers probe deeper with finer spatial resolution than visible/near-infrared remote sensing, indicating diverse hydrated sulfate minerals. For example, Mg and S abundances correlate in shallow soils at the Phoenix landing site, suggestive of Mg sulfates [e.g., *Kounaves et al.*, 2010a]. In the southern highlands, at Gusev Crater, Spirit found similar Mg-S chemistry in excavated soils developed on Hesperian (3.7 to ~3 Ga) basaltic plains [*Haskin et al.*, 2005], whereas the older Noachian Columbia Hills soils hosted localized concentrations of Fe^{3+} and Ca sulfates [*Johnson et al.*, 2007; *Lane et al.*, 2008; *Yen et al.*, 2008; *Arvidson et al.*, 2010; *Wang et al.*, 2013]. But these geographically restricted landed measurements probing depths of mostly a few centimeters leave much of Mars's southern hemisphere unexplored. Here we use orbital data, including the sulfur map of Mars, for a broader view of Martian soil hydration at hemispheric to global scales. The potential for Fe sulfate species to reflect diverse aqueous environments on Mars, due in part to the crustal abundance of Fe and S relative to Earth [e.g., *Lane et al.*, 2014], further motivates our work.

2. Data and Methods

Our study originates from the elemental mass fraction data derived from gamma ray spectrometer (GRS) γ photon spectra [*Boynton et al.*, 2007]. Corresponding S and H_2O (computed stoichiometrically from H)

in the low to middle latitudes (0 to ~45°) probe the nature of both hydrous sulfates and other hydrates throughout the uppermost decimeters (Figure S1 in the supporting information). Sensitive to regional scales over which relative rock abundances are typically low [*Karunatillake et al*., 2007], GRS observations primarily reflect the "soil" component for mobile elements such as H and S. In the context of our work, the distinction of outcrop/bedrock and other less mobile components from the finer and more mobile regolith components becomes important [*Newsom et al*., 2007], although local rocks probably contribute to a fraction of the soil [*Meslin et al*., 2013]. Following common practice in the planetary literature [*McSween et al*., 2010], we use the term soil to represent the latter component, varying in grain size from clay to cobbles on the Wentworth Scale, without biological implications [*Karunatillake et al*., 2007; *Certini and Ugolini*, 2013].

2.1. Chemical Maps of H_2O and S Mass Fractions

Years of data collection recently yielded the first preliminary midlatitudinal sulfur map [*King and McLennan*, 2010], updated further in this work, but the substantial smoothing needed for numerical precision causes spatial autocorrelation [*Karunatillake et al*., 2012] and limits our spatial resolution for the sulfur mass fraction, w(S), to the 10° × 10° bins used here. We accordingly rebinned $w(H_2O)$ from its original 5° × 5° resolution to 10° × 10°. The global data are limited to roughly ±45° because only H_2O (not S) mass fractions can be accurately inferred in the polar regions at present [*Boynton et al*., 2007].

We use two different γ peaks to determine sulfur: 5421 keV and its positron escape peak at 4911 keV. Both peaks are reasonably well resolved from their nearby neighbors, and the continuum under the peaks is well determined from regions without peaks on either side of the peaks of interest. The peak used for the H determination (2223 keV) [*Evans et al*., 2006] is very far removed from the S peaks, so spectral interference cannot explain the correlation between S and H seen in this work. We describe the S peaks further in the supporting information.

The stoichiometrically equivalent H_2O (Figure 1a) and S (Figure 1b) maps represent similar depths in the Martian regolith (Figure S1 in the supporting information). Using the standard g/cm^2 column density representation of depth [e.g., *Boynton et al*., 2007], 50% of the cumulative signal for H emerges from depths up to about 14 g/cm^2, while that of the higher-energy S peaks emerges from up to ~21 g/cm^2. We may use a bulk density of ~1.3 g/cm^3, representing the average of Martian soil (e.g., S. Karunatillake et al., Regolith models for in situ neutron and gamma instrumentation on Mars, manuscript in preparation for *Earth and Planetary Science Letters*, 2014), to compute corresponding depths. This yields ~11 cm for H and ~16 cm for S, effectively placing the sampling depth for spectral peaks corresponding to both H and S at similar, decisively deeper than surficial, depths. Accordingly, the 90% cumulative signal depth would approximate a few decimeters for both elements.

The similarity in sampling depths allows us to consider correlations driven by the chemical association of H and S in bulk soil. For the broadest possible insight into a possible spatial association between H and S, we assessed the data in two key ways: (1) bivariate regression and correlation globally and hemispherically in the midlatitudes, with the latter helping to reveal any differences corresponding roughly with the planetary age topography dichotomy, and (2) kernel density estimated (KDE) histograms of stoichiometric H_2O to S molar ratios, not only for consistency with correlation results but also for consistency with particular mineral phases.

2.2. Regression and Correlation

To examine the strength of the relationship between water and sulfur mass fractions, $w(H_2O)$ and w(S), we computed linear regression fits to the GRS data: $w(H_2O) = m \times w(S) + C$, where m represents the stoichiometric association between H_2O and S. Related calculations rely on a robust spatial statistics/geographic information system methodology [*Karunatillake et al*., 2012] within which, in the context of Figure 2, R^2 identifies the proportion of H_2O variance that can be modeled with sulfur alone, while r reflects the strength of the correlation. If a statistically significant linear fit does not exist, we may model all the H_2O bound to nonsulfates, with the H_2O content merely providing an upper bound on the mass fraction of hydrous sulfates. This changes if the data show that S alone can model the variance of H_2O, particularly if the correlation coefficient is nonzero at 95% confidence. If so, the model fit intercept, C, would show the excess or deficit in H_2O relative to its observed variation with S. A positive intercept then suggests the availability of H_2O for non-S modes, while a negative intercept reveals the lack of sufficient H_2O to model with available S. We report the uncertainty

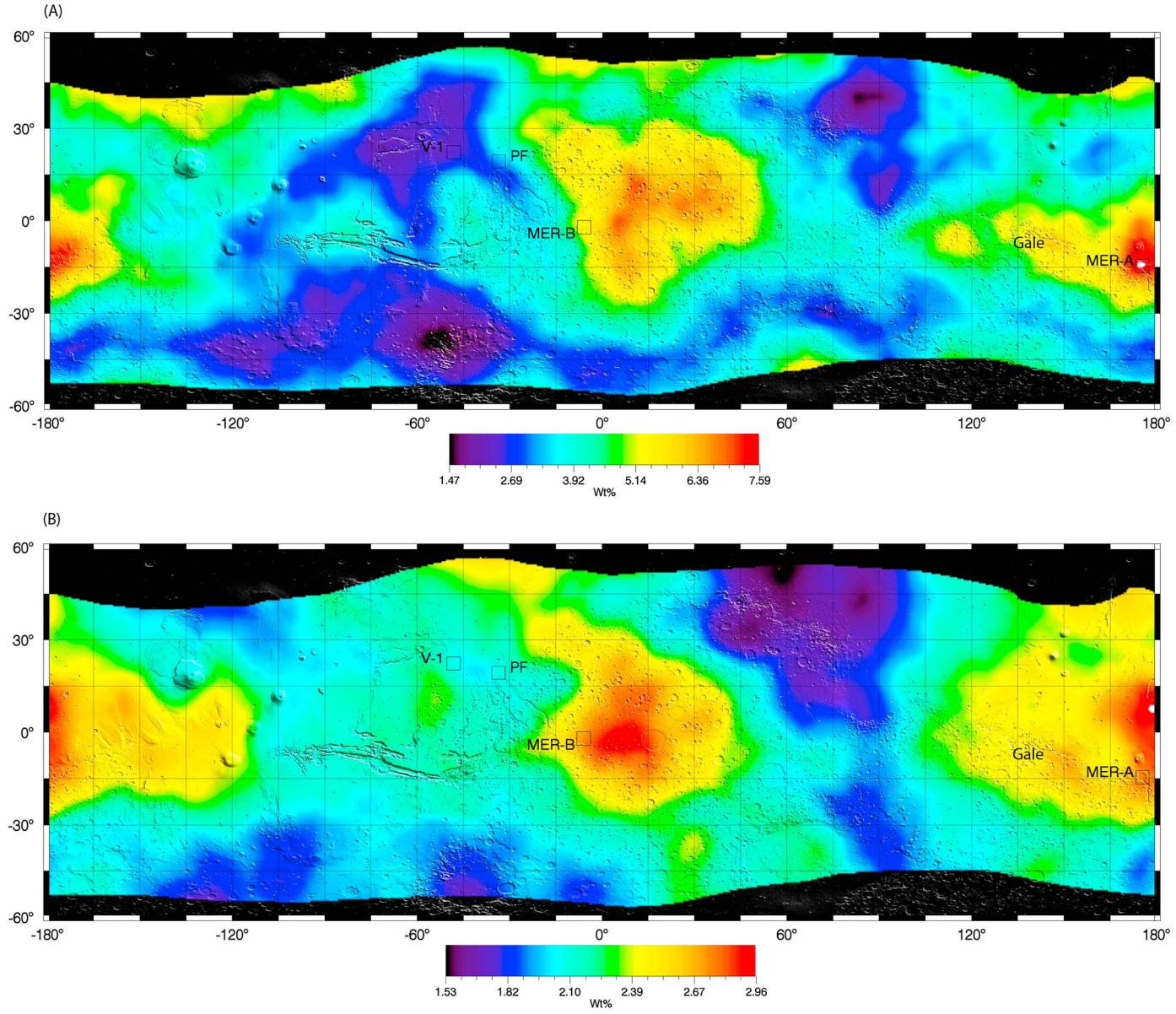

Figure 1. (a) Map of stoichiometrically equivalent H_2O mass fractions as percentage, $w(H_2O)$, derived from GRS γ spectroscopy. Equirectangular projection uses east longitude notation. Scale bar at bottom indicates the color-coded $w(H_2O)$ values, which range from 1% to 8% within the $5° \times 5°$ spatial resolution limit. Overlain on Mars Orbiter Laser Altimeter-derived topography with landing sites identified as V-1 (Viking 1), PF (Pathfinder), MER-B (Opportunity Rover at Meridiani), MER-A (Spirit Rover at Gusev), and Gale (Curiosity Rover). Black hue defines the boundary of chemical data. (b) Map of stoichiometrically equivalent S mass fractions as percentage, $w(S)$, derived from GRS γ spectroscopy. Scale bar at bottom color codes $w(S)$ values, which range from 1% to 3% (stoichiometrically equivalent to 2.5% to 7.5% of SO_3) within the $10° \times 10°$ spatial resolution limit.

of each parameter, with the exception of R^2, to one standard error. Of note, chemical data cannot distinguish between hydroxylation and hydration, so we include both among candidate minerals (Table S1 in the supporting information). Lastly, correlative methods can establish consistency, though not causation. These caveats underlie the model we develop subsequently of bulk soil hydration.

2.3. Kernel Density Estimated Histogram

The molar ratio of H_2O to S—termed hydration state for brevity—across Mars helps to constrain hydrous sulfates that may underpin observed correlations between H_2O and S. We used kernel density estimation (KDE) to generate the frequency histogram in Figure 3 of midlatitudinal global hydration states. For hydration states corresponding spatially to nearly constant area pixels, the KDE histogram (Figure 3) visualizes the probability

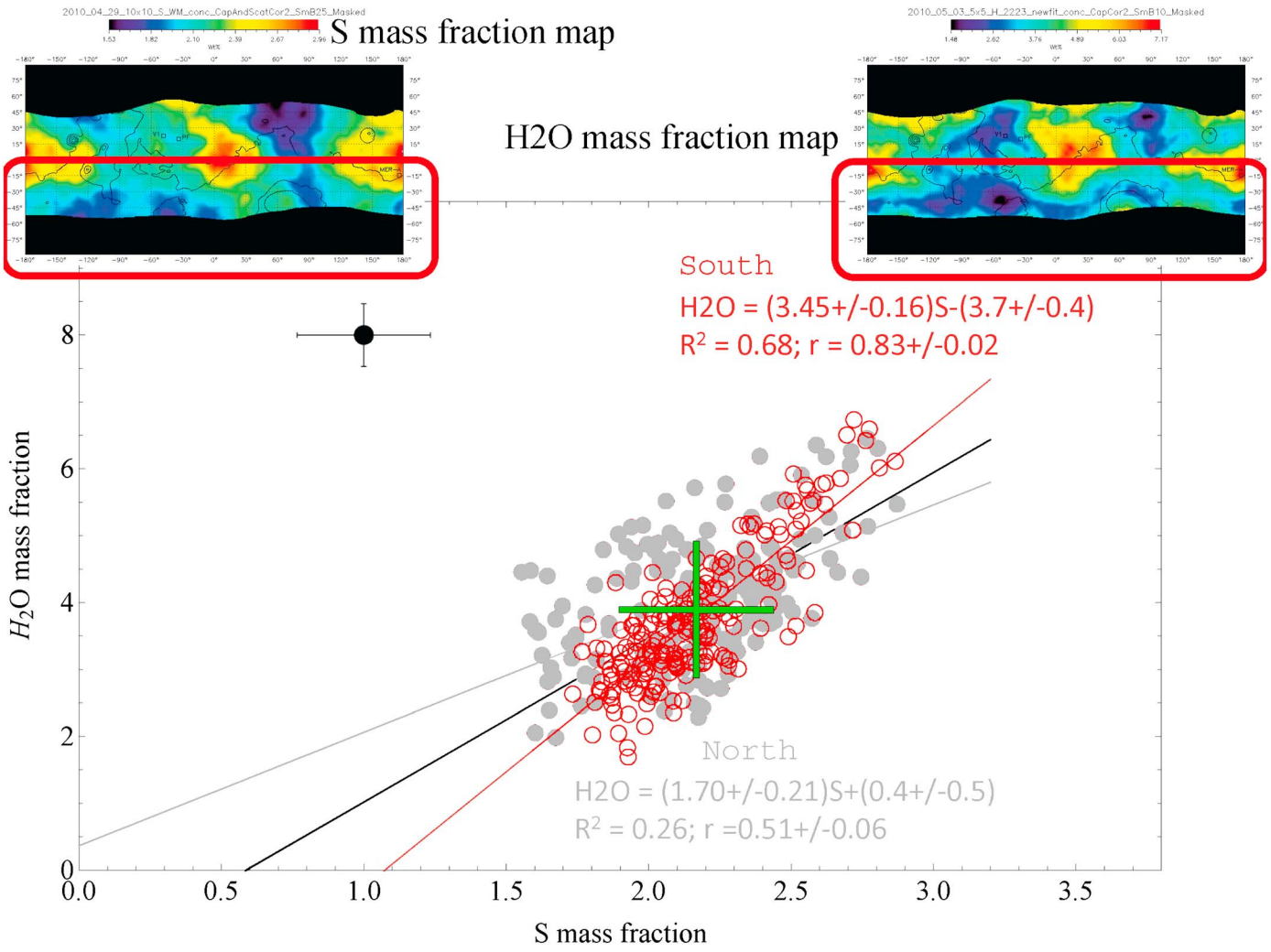

Figure 2. Correlation between GRS $w(H_2O)$ and $w(S)$ in the low and middle latitudes. Chemical map thumbnails shown as insets (S on the left and H on the right, as labeled) to visually summarize the underlying data across Mars, with high-resolution versions as Figures 1a and 1b. The southern hemisphere data are red circles, while the northern hemisphere data are shown as light gray dots. The global regression line, in black, is intermediate between those of the northern and southern hemispheres. The average global values and their standard deviations are indicated by the green cross. Typical numerical uncertainties for a single data point (computed as the root-mean-square of global uncertainties) are shown by error bars in the top left. Actual uncertainties are likely smaller, because the data have been binned to coarser resolution. Uncertainties shown for the regression parameters are one standard error. Note the strong correlation and negative intercept of the southern hemisphere regression line.

density function of the underlying pixel frequency distribution. That is, the number of pixels binned across infinitesimally small value range on the continuum of hydration states. Consequently, the area under the histogram corresponds approximately to the relative area of the Martian surface in the low and middle latitudes.

The superiority of KDE relative to other histograms stems from its properties. For example, KDE enables peaks in the sample distribution to be distinguished visually above noise. As a nonparametric method, KDE also reveals the nature of the overall distribution without bias from assumed population distributions. As previously used in planetary science [e.g., *Gasnault et al.*, 2010], KDE enhances insight into spatial data, and the method remains both critical and mature in fields as diverse as signal processing [*Liu et al.*, 2009], econometrics [*Bouezmarni and Scaillet*, 2005], automated visual surveillance [*Elgammal et al.*, 2002], and neuroscience [*Shimazaki and Shinomoto*, 2010].

The kernel density estimator takes the form $f_w(y) = \frac{1}{nw}\sum_{j=1}^{n} K\left(y - y_j/w\right)$, where K denotes the kernel function (Gaussian in our case), n the number of data, w the bandwidth, and y the input values (hydration

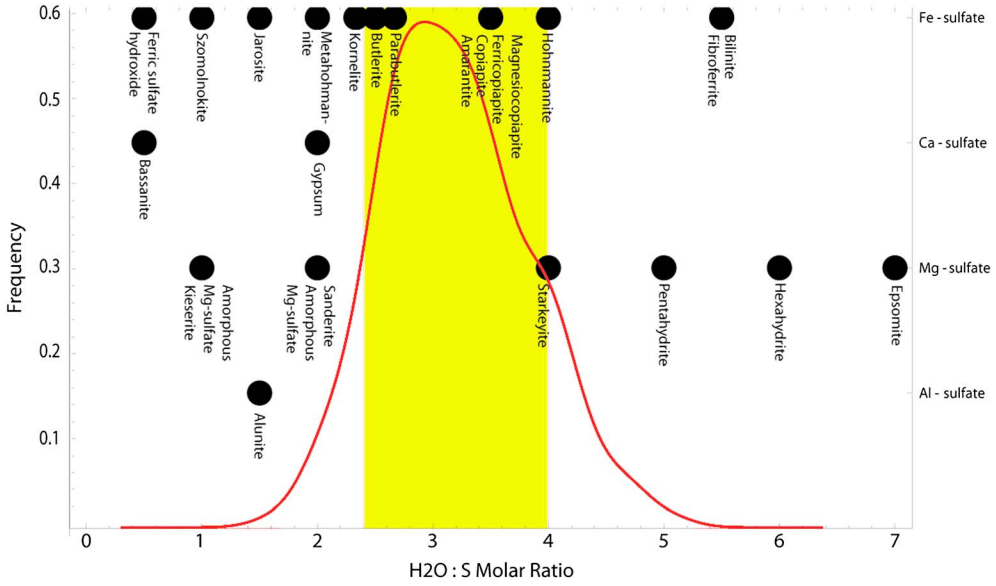

Figure 3. Pixel frequency distribution represented by the probability density function (left ordinate scale labeled "frequency") of low to middle latitude hydration states (H_2O:S molar ratio) from GRS (abscissa), processed with a Gaussian kernel density estimation (section 2.3). Hydration states between 2.4 and 4 characterize ~80% of the shallow subsurface as indicated by the area beneath the histogram. Each candidate sulfate from Table S1 is plotted according to its hydration state (horizontal axis) and primary cation (vertical position, with key at right). The observed distribution is best explained by the sulfates within the yellow peak region, populated by Fe sulfates that are all of the chain sulfate variety [*Hawthorne et al.*, 2000].

state in our case). We adapted a standard KDE plot algorithm developed by *Hamrick* [2008] that identifies subdistributions uniformly at a given bandwidth across data of varying dynamic range. Furthermore, instead of computationally optimizing [*Sheather and Jones*, 1991] the smoothing parameter, KDE bandwidth (w), we varied w continuously between 0.2 and 2—the standard dynamic range of w—to assess the hydration state distribution robustly. Comparison of outcomes with other kernels, including triangular, uniform, and triweight, suggested more informative results with the Gaussian kernel. This also converges with the common use of a Gaussian kernel in the literature.

3. Results and Discussion

We present the global regression correlation (section 2.2) results summarily in Figure 2, with the three large-scale analyses identified by three colors described in the figure caption. We also summarize the global H_2O and S mass fraction distributions using the variance (represented by the standard deviation in Figure 2) and mean. Additionally, the conservative numerical uncertainty of a datum on average—computed as the root-mean-square of global uncertainties—is represented with error bars to one standard error (Figure 2, top left). This per datum numerical uncertainty does not exceed the variance of H_2O and S (Figure 2, green cross), indicating robust regression results.

The global regression represents the nature of H_2O and S covariance in the bulk soil throughout the midlatitudes (Figure 2). The corresponding negative C (Figure 2) indicates the possibility for all H_2O to be chemically bound to S throughout the midlatitudinal bulk soil. Nevertheless, the correlation coefficient, r, of 0.58 ± 0.06 at 95% confidence, as well as $R^2 = 0.43$, suggests considerable distributional scatter weakening the association between H_2O and S or that the relationship is more regional than global. Accordingly, we examine the possibility of globally dichotomous associations with the insight afforded by southern and northern hemispheric analyses. Large areas must be considered to ensure statistical robustness. This ensures that the variance of H_2O and S exceeds their respective root-mean-square uncertainties: about 0.5% (absolute) for H_2O and about 0.2% (absolute) for S (Figure 2).

Our work in bivariate space with H_2O and S marks the initial step to motivate multivariate analyses across all elements derived from γ spectra. Nevertheless, prior work identifies multivariate associations among Cl, H, K,

Si, Th, albedo, rock areal fraction, surface type 1 areal fraction, surface type 2 areal fraction, and thermal inertia [*Karunatillake et al*., 2006, 2012]. Based on those analyses, we identify Cl as the only variable that may modify the model built on S and H. Given that Cl variation can only model about 20% of H variation in multivariate space [*Karunatillake et al*., 2006, Table 2], we anticipate that only negligible to minor changes of our bivariate observations would result from analyses in Cl, H, and S multivariate space.

3.1. Sulfates Hydrating Bulk Soil

Regression correlation (section 2.2) yields a negative *C* for the southern hemisphere (Figure 2), revealing the feasibility of modeling all H_2O as bound chemically to sulfates. The negative *C* allows the presence of anhydrous S in forms such as sulfides, anhydrite, and adsorbed to nanophase ferric grains, each consistent with rover results from the low southern latitudes [*Morris et al*., 2006; *Nachon et al*., 2013; *McAdam et al*., 2014]. Reinforcing the absence of excess H_2O, we may model 68% of H_2O variability (R^2) with S alone in the southern highlands, where the dust cover index tends to be lower [*Ruff and Christensen*, 2002].

In particular, the strong correlation coefficient (0.83 ± 0.04 at 95% confidence) of H_2O with S in the south, along with the absence of excess H_2O (Figure 2), does not require grain adsorption, specific surface area, or porosity [*Milliken et al*., 2007; *Jänchen et al*., 2009] as dominant controls on subsurface hydration, at least at the regional scale sensed by GRS. However, previously observed negative correlation between atmospheric water vapor content and regional thermal inertia [*Beck et al*., 2010] suggests an association of H_2O with fine grains. This is supported by Chemical Camera observations at Gale that reveals a ubiquitous hydrogen signature in the first centimeter of fine soil [*Meslin et al*., 2013], although this hydration level may not be unique at this landing site [*Cousin et al*., 2014; *Schröder et al*., 2014]. Despite the approximately millimeter-centimeter thickness of recent laboratory assessment of Martian regolith adsorption cycles with H_2O [*Beck et al*., 2010; *Massé et al*., 2014], nearly 2 orders of magnitude smaller than γ sampling depths, adsorption may also play a role in bulk soil hydration [*Jänchen et al*., 2009]. We may reconcile this with our result if adsorption cycles at the surface create a surficial link between humidity and thermal inertia, partially decoupled from the decimeter depths probed by GRS [cf. *Wang et al*., 2013]. Recent analyses of visible/near-infrared reflectance spectra globally across Mars also support a negligible role for H_2O adsorption in the Martian surface compared to chemically bound H_2O [*Audouard et al*., 2014].

In the northern hemisphere, the correlation—computed as described in section 2.2—between $w(H_2O)$ and $w(S)$ is weaker, and regression intercept *C* is slightly positive approximating 10% of average $w(H_2O)$ (Figure 2), indicating that this fraction may not associate with structural H in sulfates. Consistent with this result, the higher dust cover index in the north [*Ruff and Christensen*, 2002] may enable a meaningful role for microtexture and specific surface area in the distribution of H_2O, independent of mineralogy. Nonsulfate hydrates may also contribute to the weaker correlation ($r = 0.51$) between H and S in the northern hemisphere, even though visible/near-infrared spectroscopy detects such minerals predominantly in the southern hemisphere and in craters elsewhere [e.g., *Carter et al*., 2013]. Furthermore, the weaker correlation in the northern hemisphere may reflect collocation in various regolith components (rocks versus soil and crystalline versus amorphous) without chemical association. The presence of peroxides in the regolith [e.g., *Encrenaz et al*., 2012; *Glavin et al*., 2013] may weaken the association of H with S as well. Alternatively, sulfates may simply have more variable hydration in the north, consistent with prior interpretations of Mars Odyssey Neutron Spectrometer data [*Fialips et al*., 2005]. That said, the rough compositional constraints we develop for sulfates with GRS data in section 3.2 do not suggest comparable abundances of diversely hydrated sulfates.

Regression at the finest latitudinal resolution possible across the entire planet supports the regional observations. To ensure statistical robustness [cf. *Karunatillake et al*., 2012], we chose 10° wide bands, each usually containing 36 values. The strengths of correlations are similar at latitudes beyond ~±40°, with H_2O and S correlation weakening below *r* values of 0.2 at bands centered at ±55°. This weakening appears to begin at ±45°. However, a hemispheric dichotomy in H_2O and S association, with strongest coupling in the southern hemisphere, also remains apparent. For example, most southern latitudinal bands manifest *r* values no less than 0.60, while most northern bands remain below 0.60. Accordingly, at both the coarsest hemispheric scale discussed previously and the finest statistically sound latitudinal resolution of the instrument, we find a convincing possibility of H_2O associated with S in bulk soil of the southern hemisphere.

Our observations, suggesting hydrous sulfates as a key carrier of southern midlatitudinal H_2O, offer an alternative to prior suggestions that the shallow subsurface may contain widespread phyllosilicates [*Noe Dobrea et al.*, 2010] and zeolites [*Bish et al.*, 2003] or that water ice accounts for a significant fraction of low-latitude H_2O [*Jakosky et al.*, 2005]. Correlation does not imply causation, especially in bivariate analyses. However, the ease of decoupling H_2O and S that could result from the many phases and processes that affect their variations independently makes the strong spatial correlation we observe ($r = 0.83$) chemically compelling. The remarkable contrast between north and south in the association of H_2O and S (Figure 2) reinforces this further, particularly in the context of older exposed terrain and less fine debris mantles in the south.

3.2. Hydrous Sulfate Compositional Insight

Next we compare the global distribution of sulfate "hydration states" (defined as the H_2O:S molar ratio) to a comprehensive library of sulfates expected on Mars based on orbital and in situ observations, thermodynamic models, and hydration-dehydration experiments under Mars-like conditions (Figure 3, with choice of sulfates described in Table S1 in the supporting information). By relying on the stoichiometric feasibility of compositions, this approach avoids misattribution that could result from absolute abundances of H_2O and S. We avoid an exhaustive library of minerals. Instead, a judicious comparison with reasonable hydrous mineral candidates on Mars, especially those observed in situ in bulk soil which may best relate to GRS data (section 2), provides optimal insight. This applies particularly given the elemental, as opposed to mineralogic, hemispheric perspective we develop for bulk soil. Our 27 candidate sulfates have 13 distinct hydration states (Table S1) that span the range of values observed by GRS and beyond (Figure 3).

The weaker association of H_2O and S in some areas, especially in the northern hemisphere (Figure 2), does not disrupt global trends in hydration state (Figure 3). A comparison of hydration state distributions both with histograms and with summary parameters between the two hemispheres, including variations across latitudinal bands, suggests broadly comparable hydration states. Subtle differences arise in the detailed variation. However, the weak association of H_2O and S (Figure 2) precludes meaningful compositional constraints in the north. In contrast, the constraints we develop subsequently apply meaningfully in the south given the compelling association between H_2O and S. The general absence of fine debris in the south, such as dust mantles, which may suppress underlying chemical hydration signatures, lends additional support.

The global hydration states show a nearly normal distribution (Figure 3). Varying w continuously across the entire 0.2 to 2.0 range demonstrates this first. By visualizing how KDE histograms vary throughout the range of w, we avoided pitfalls of subsampling as may result from optimizing w computationally [cf. *Sheather and Jones*, 1991]. Even at the lowest bandwidth ($w = 0.2$) of minimal processing, the distribution assumes the approximately unimodal nature evident in Figure 3. The slight shoulder at hydration 4.0 disappears when w increases to 0.3, making the distribution indistinguishable from a normal distribution. Throughout the w variation between 0.2 and 2, the distribution preserves the peak at hydration ~3.

Had several distinct hydration states been present in globally significant quantities, multimodality, platykurty, or substantial skewness would have resulted, unlike the distribution we observe (Figure 3). For example, *Gasnault et al.*'s [2010, Figure 3] use of an identical KDE revealed the subpeaks and shoulders for some of the elemental mass fraction distributions. This also demonstrates that GRS data ably reveal regional-scale variations despite the spatial autocorrelation [e.g., *Karunatillake et al.*, 2012] induced by coarse [*Boynton et al.*, 2007] lateral resolution.

We may use the nature of the hydration state distribution to roughly constrain the composition of sulfates. The slight shoulder at 4.0 hydration (Figure 3), visible only for the least processing ($w = 0.2$), demarcates the 90th percentile. The 10th percentile corresponds to 2.4. Given the normality of the distribution with barely a positive skewness (Figure 3), the range between the 10th and 90th percentiles corresponds directly to distributional area and consequently to 80% of the midlatitudinal area. Higher and lower hydration values represent less than 20% of the subsurface. Specifically, the implicit low abundance of lower and higher hydration in the KDE histogram decreases the likelihood of the corresponding minerals constituting bulk soil at regional scales. Furthermore, a single mineral type dominating bulk soil hydration would yield the unimodal Gaussian shape of the distribution more consistently than a mixture of diversely hydrated phases.

Modeling the observed hydration with Mg and Ca sulfates requires several assumptions. First, highly hydrated Mg sulfates would need to coexist with weakly hydrated Ca sulfates, none of which exceeds H_2O:S ~ 2 (Figure 3). Such mixtures must also exist throughout the regional scales and decimeter depths sensed by the GRS to generate an observable signature such as the association of H with S. The thermodynamic stability range of anhydrite ($CaSO_4$) does overlap with that of hexahydrite ($MgSO_4 \cdot 6H_2O$) [*Chou and Seal*, 2007]; to obtain H_2O:S ~ 3 (Figure 3) would then require similar proportions of Ca and Mg sulfates. However, observations at Gale Crater raise the possibility of various amorphous phases controlling the hydration of the fine-grained soil component [*Cousin et al*., 2014; *McAdam et al*., 2014]. Furthermore, other landing sites, where Mg sulfates dominate over Ca sulfates [*Vaniman et al*., 2004; *Kounaves et al*., 2010b], would require a mixture of metastable starkeyite with anhydrite, kieserite, or amorphous Mg sulfates. At the surface, such mixtures may experience disequilibrium when relative humidity increases above ~20% each evening [*Savijärvi*, 1995]. Subsurface mixing or stratification may exist, provided they preserve the observed bulk H and S trends while maintaining a dynamic equilibrium with humidity and temperature gradients that may exist in the soil profile [cf. *Wang and Ling*, 2011].

Mg sulfates, although suggested as the dominant soil sulfates based on chemical data at many Mars landing sites [*Vaniman et al*., 2004; *Kounaves et al*., 2010a, 2010b], generally do not exhibit hydration in the 2.4 to 4 range aside from the metastable phases starkeyite ($MgSO_4 \cdot 4H_2O$) and the recently discovered 2.5 hydrate [*Ma et al*., 2009]. Several recent studies suggest that Martian conditions may enhance starkeyite stability [*Chipera and Vaniman*, 2007; *Chou and Seal*, 2007; *Wang et al*., 2009; *Steiger et al*., 2011], and the inflection near hydration state 4 in our distribution (Figure 3) might indicate the importance of this mineral in certain regions [cf. *Liu et al*., 2012]. However, the peak at H_2O:S ~ 3 in our unimodal distribution (Figure 3) not only lacks corresponding crystalline Mg sulfates but also represents the maximum possible hydration for amorphous Mg sulfates [*Wang et al*., 2009].

Could we attribute the range of hydration suggested by the global KDE histogram simply to one mineral group? Unlike Mg and Ca sulfates that require complex mixtures at hydration extremes, several Fe sulfates hydrate between 2.4 and 4 (Figure 3 and Table S1). The iron in these sulfates is mostly Fe^{3+}, with specific candidates including butlerite, (ferri)copiapite, amarantite, and hohmannite, all considered possible constituents of the Paso Robles class soils identified in the shallow subsurface in Spirit's wheel trenches [*Johnson et al*., 2007; *Lane et al*., 2008; *Yen et al*., 2008; *Lane*, 2014]. The compositional convergence with Paso Robles-type soil matters, because it represents a subsurface composition that γ spectra may also sample regionally to decimeter depths. The mineralogic insensitivity of our data and the regional perspective preclude a robust distinction between complex mixtures of minerals versus a central role to a single mineral. However, hydrous Fe^{3+} sulfates, as a carrier of H_2O in the midlatitudinal bulk Martian soil, would explain the observed hydration distribution without the complexity posed by Ca/Mg or Mg/Mg sulfate mixture alternatives.

4. Conclusions and Future Work

Our observations of covarying S and H_2O support a central role for hydrous sulfates in driving the distribution of H_2O in the southern midlatitudes of Mars. This applies specifically for bulk soil at decimeter depths, including the speculation that genetic processes of Fe sulfate-rich Paso Robles soil in Gusev Crater may have been more widespread at regional scales in more ancient terrain of Mars than previously appreciated. However, the elemental nature of the underlying data and reliance on correlation preclude specificity of sulfate cations. Future work assessing the latitudinal variation of hydration states; characterizing regions mantled by fine debris; and comparing across H_2O- and S-enriched and depleted regions will help refine our model. Ongoing observations of bulk soil by the Curiosity Rover at Gale Crater may constrain the relevance of our model to Martian aqueous processes.

In addition, laboratory analyses of Fe^{3+} sulfate thermodynamics and detailed characterization of recurring slope lineae growth rates in the Martian southern hemisphere may provide important independent constraints on the likelihood of widespread Fe^{3+} sulfates on Mars. Specifically, warm-season growth rates vary inversely with fluid viscosity [*Levy*, 2012]. At low temperatures, concentrated Fe^{3+} sulfate brines can be 6 orders of magnitude more viscous than H_2O and 2 orders of magnitude more than chloride or Mg sulfate brines [*Chevrier et al*., 2009], implying uniquely low growth rates and the potential to resolve sulfate cation uncertainties using only orbital imagery.

Acknowledgments

We thank our two reviewers, Melissa Lane and Selby Cull, for suggestions that improved the robustness and clarity of our work. We also thank D. Hamara and the Mars Odyssey GRS team for collegial support. B. Sutter, D. Archer, A.A. Pavlov, and A. Wang provided insight by asking perceptive questions, while Chris C. Diaz and Donald Hood aided in revisions. This research was supported by NASA/Jet Propulsion Lab (Mars Odyssey GRS instrument): by NASA Mars Data Analysis Program grants NNX07AN96G and NNX10AQ23G to S.M.M., by NASA MDAP grant NNX12AG89G/NNX13AI98G to S.K., by CNES and CNRS support to O.G., and by LSU's Geology and Geophysics post-doctoral support to J.R.S. The underlying data are available at the PDS and the Mars Odyssey GRS website (upon request).

Andrew Dombard thanks Melissa Lane and Selby Cull for their assistance in evaluating this paper.

References

Arvidson, R. E., et al. (2010), Spirit Mars Rover Mission: Overview and selected results from the northern Home Plate Winter Haven to the side of Scamander crater, *J. Geophys. Res.*, *115*, E00F03, doi:10.1029/2010JE003633.

Audouard, J., F. Poulet, M. Vincendon, R. E. Milliken, D. Jouglet, J. Bibring, B. Gondet, and Y. Langevin (2014), Water in the Martian regolith from OMEGA/Mars Express, *J. Geophys. Res. Planets*, *119*, 1969–1989, doi:10.1002/2014JE004649.

Beck, P., A. Pommerol, B. Schmitt, and O. Brissaud (2010), Kinetics of water adsorption on minerals and the breathing of the Martian regolith, *J. Geophys. Res.*, *115*, E10011, doi:10.1029/2009JE003539.

Bish, D. L., J. William Carey, D. T. Vaniman, and S. J. Chipera (2003), Stability of hydrous minerals on the Martian surface, *Icarus*, *164*(1), 96–103, doi:10.1016/S0019-1035(03)00140-4.

Bouezmarni, T., and O. Scaillet (2005), Consistency of asymmetric kernel density estimators and smoothed histograms with application to income data, *Econ. Theory*, *21*, 390–412, doi:10.1017/S0266466605050218.

Boynton, W. V., et al. (2007), Concentration of H, Si, Cl, K, Fe, and Th in the low- and mid-latitude regions of Mars, *J. Geophys. Res.*, *112*, E12S99, doi:10.1029/2007JE002887.

Carter, J., F. Poulet, J.-P. Bibring, N. Mangold, and S. L. Murchie (2013), Hydrous minerals on Mars as seen by the CRISM and OMEGA imaging spectrometers: Updated global view, *J. Geophys. Res. Planets*, *118*, 831–858, doi:10.1029/2012JE004145.

Certini, G., and F. C. Ugolini (2013), An updated, expanded, universal definition of soil, *Geoderma*, *192*, 378–379, doi:10.1016/j.geoderma.2012.07.008.

Chevrier, V. F., R. Ulrich, and T. S. Altheide (2009), Viscosity of liquid ferric sulfate solutions and application to the formation of gullies on Mars, *J. Geophys. Res.*, *114*, E06001, doi:10.1029/2009JE003376.

Chipera, S. J., and D. T. Vaniman (2007), Experimental stability of magnesium sulfate hydrates that may be present on Mars, *Geochim. Cosmochim. Acta*, *71*(1), 241–250, doi:10.1016/j.gca.2006.07.044.

Chou, I.-M., and R. R. Seal II (2007), Magnesium and calcium sulfate stabilities and the water budget of Mars, *J. Geophys. Res.*, *112*, E11004, doi:10.1029/2007JE002898.

Cousin, A., et al. (2014), Compositions of coarse and fine particles in Martian soils at Gale: A window into the production of soils, *Icarus*, doi:10.1016/j.icarus.2014.04.052.

Elgammal, A., R. Duraiswami, D. Harwood, and L. S. Davis (2002), Background and foreground modeling using nonparametric kernel density estimation for visual surveillance, *Proc. IEEE*, *90*(7), 1151–1163, doi:10.1109/JPROC.2002.801448.

Encrenaz, T., T. K. Greathouse, F. Lefèvre, and S. K. Atreya (2012), Hydrogen peroxide on Mars: Observations, interpretation and future plans, *Planet. Space Sci.*, *68*(1), 3–17, doi:10.1016/j.pss.2011.03.019.

Evans, L. G., R. C. Reedy, R. D. Starr, K. E. Kerry, and W. V. Boynton (2006), Analysis of gamma ray spectra measured by Mars Odyssey, *J. Geophys. Res.*, *112*, E03S04, doi:10.1029/2005JE002657.

Feldman, W. C., et al. (2004), Hydrated states of $MgSO_4$ at equatorial latitudes on Mars, *Geophys. Res. Lett.*, *31*, L16702, doi:10.1029/2004GL020181.

Fialips, C. I., J. W. Carey, D. T. Vaniman, D. L. Bish, W. C. Feldman, and M. T. Mellon (2005), Hydration state of zeolites, clays, and hydrated salts under present-day Martian surface conditions: Can hydrous minerals account for Mars Odyssey observations of near-equatorial water-equivalent hydrogen?, *Icarus*, *178*(1), 74–83, doi:10.1016/j.icarus.2005.04.020.

Gasnault, O., G. Jeffrey Taylor, S. Karunatillake, J. Dohm, H. E. Newsom, O. Forni, P. Pinet, and W. V. Boynton (2010), Quantitative geochemical mapping of Martian elemental provinces, *Icarus*, *207*(1), 226–247, doi:10.1016/j.icarus.2009.11.010.

Glavin, D. P., et al. (2013), Evidence for perchlorates and the origin of chlorinated hydrocarbons detected by SAM at the Rocknest aeolian deposit in Gale Crater, *J. Geophys. Res. Planets*, *118*, 1955–1973, doi:10.1002/jgre.20144.

Hamrick, J. (2008), Kernel density estimation, Wolfram Demonstr. Proj. [Available at http://demonstrations.wolfram.com/KernelDensityEstimation/.]

Haskin, L. A., et al. (2005), Water alteration of rocks and soils on Mars at the Spirit rover site in Gusev Crater, *Nature*, *436*(7047), 66–69, doi:10.1038/nature03640.

Hawthorne, F. C., S. V. Krivovichev, and P. C. Burns (2000), The crystal chemistry of sulfate minerals, *Rev. Mineral. Geochem.*, *40*(1), 1–112, doi:10.2138/rmg.2000.40.1.

Jakosky, B., M. Mellon, E. Varnes, W. Feldman, W. V. Boynton, and R. Haberle (2005), Mars low-latitude neutron distribution: Possible remnant near-surface water ice and a mechanism for its recent emplacement, *Icarus*, *175*(1), 58–67, doi:10.1016/j.icarus.2004.11.014.

Jänchen, J., R. V. Morris, D. L. Bish, M. Janssen, and U. Hellwig (2009), The H_2O and CO_2 adsorption properties of phyllosilicate-poor palagonitic dust and smectites under Martian environmental conditions, *Icarus*, *200*(2), 463–467, doi:10.1016/j.icarus.2008.12.006.

Johnson, J. R., J. F. Bell III, E. Cloutis, M. Staid, W. H. Farrand, T. McCoy, M. Rice, A. Wang, and A. S. Yen (2007), Mineralogic constraints on sulfur-rich soils from Pancam spectra at Gusev Crater, Mars, *Geophys. Res. Lett.*, *34*, L13202, doi:10.1029/2007GL029894.

Karunatillake, S., et al. (2006), Composition of northern low-albedo regions of Mars: Insights from the Mars Odyssey Gamma Ray Spectrometer, *J. Geophys. Res.*, *112*, E03S05, doi:10.1029/2006JE002675.

Karunatillake, S., J. M. Keller, S. W. Squyres, W. V. Boynton, J. Brückner, D. M. Janes, O. Gasnault, and H. E. Newsom (2007), Chemical compositions at Mars landing sites subject to Mars Odyssey Gamma Ray Spectrometer constraints, *J. Geophys. Res.*, *112*, E08S90, doi:10.1029/2006JE002859.

Karunatillake, S., O. Gasnault, S. W. Squyres, J. M. Keller, D. M. Janes, W. V. Boynton, and H. E. Newsom (2012), Martian case study of multivariate correlation and regression with planetary datasets, *Earth Moon Planets*, *108*, 253–273, doi:10.1007/s11038-012-9395-x.

King, P. L., and S. M. McLennan (2010), Sulfur on Mars, *Elements*, *6*(2), 107–112, doi:10.2113/gselements.6.2.107.

Kounaves, S. P., et al. (2010a), Soluble sulfate in the Martian soil at the Phoenix landing site, *Geophys. Res. Lett.*, *37*, L09201, doi:10.1029/2010GL042613.

Kounaves, S. P., et al. (2010b), Wet Chemistry experiments on the 2007 Phoenix Mars Scout Lander mission: Data analysis and results, *J. Geophys. Res.*, *115*, E00E10, doi:10.1029/2009JE003424.

Lane, M. D. (2014), Habitable environments include acidic zones: Looking beyond an alkaline environment for signatures of life on Mars, in *8th International Conference on Mars*, p. 1465.

Lane, M. D., J. L. Bishop, M. Darby Dyar, P. L. King, M. Parente, and B. C. Hyde (2008), Mineralogy of the Paso Robles soils on Mars, *Am. Mineral.*, *93*(5-6), 728–739, doi:10.2138/am.2008.2757.

Lane, M. D., J. L. Bishop, M. D. Dyar, T. Hiroi, S. A. Mertzman, D. L. Bish, P. L. King, and A. D. Rogers (2014), Mid-infrared emission spectroscopy and visible/near-infrared reflectance spectroscopy of Fe-sulfate minerals, *Am. Mineral.*, doi:10.2138/am.2014.4762.

Levy, J. (2012), Hydrological characteristics of recurrent slope lineae on Mars: Evidence for liquid flow through regolith and comparisons with Antarctic terrestrial analogs, *Icarus*, *219*(1), 1–4, doi:10.1016/j.icarus.2012.02.016.

Liu, X., Q. Song, and P. Li (2009), A parabolic detection algorithm based on kernel density estimation, in *Emerging Intelligent Computing Technology and Applications*, edited by D.-S. Huang et al., pp. 405–412, Springer, Heidelberg, Berlin.

Liu, Y., R. E. Arvidson, M. J. Wolff, M. T. Mellon, J. G. Catalano, A. Wang, and J. L. Bishop (2012), Lambert albedo retrieval and analyses over Aram Chaos from OMEGA hyperspectral imaging data, *J. Geophys. Res.*, *117*, E00J11, doi:10.1029/2012JE004056.

Ma, H., D. L. Bish, H.-W. Wang, and S. J. Chipera (2009), Structure determination of the 2.5 hydrate $MgSO_4$ phase by simulated annealing, *Am. Mineral.*, *94*(7), 1071–1074, doi:10.2138/am.2009.3221.

Massé, M., P. Beck, B. Schmitt, A. Pommerol, A. McEwen, V. Chevrier, O. Brissaud, and A. Séjourné (2014), Spectroscopy and detectability of liquid brines on Mars, *Planet. Space Sci.*, *92*, 136–149, doi:10.1016/j.pss.2014.01.018.

McAdam, A. C., et al. (2014), Sulfur-bearing phases detected by evolved gas analysis of the Rocknest aeolian deposit, Gale Crater, Mars, *J. Geophys. Res. Planets*, *119*, 373–393, doi:10.1002/2013JE004518.

McSween, H. Y., I. O. McGlynn, and A. D. Rogers (2010), Determining the modal mineralogy of Martian soils, *J. Geophys. Res.*, *115*, E00F12, doi:10.1029/2010JE003582.

Meslin, P.-Y., et al. (2013), Soil diversity and hydration as observed by ChemCam at Gale Crater, Mars, *Science*, *341*(6153), doi:10.1126/science.1238670.

Milliken, R. E., J. F. Mustard, F. Poulet, D. Jouglet, J.-P. Bibring, B. Gondet, and Y. Langevin (2007), Hydration state of the Martian surface as seen by Mars Express OMEGA: 2. H_2O content of the surface, *J. Geophys. Res.*, *112*, E08S07, doi:10.1029/2006JE002853.

Morris, R. V., et al. (2006), Mössbauer mineralogy of rock, soil, and dust at Gusev Crater, Mars: Spirit's journey through weakly altered olivine basalt on the plains and pervasively altered basalt in the Columbia Hills, *J. Geophys. Res.*, *111*, E02S13, doi:10.1029/2005JE002584.

Nachon, M., et al. (2013), Sulfate calcium veins observed by the ChemCam instrument onboard Curiosity, *Proc. Europ. Planet. Sci. Congr.*, *8*, 8–13.

Newsom, H. E., et al. (2007), Geochemistry of Martian soil and bedrock in mantled and less mantled terrains with gamma ray data from Mars Odyssey, *J. Geophys. Res.*, *112*, E03S12, doi:10.1029/2006JE002680.

Noe Dobrea, E. Z., et al. (2010), Mineralogy and stratigraphy of phyllosilicate-bearing and dark mantling units in the greater Mawrth Vallis/west Arabia Terra area: Constraints on geological origin, *J. Geophys. Res.*, *115*, E00D19, doi:10.1029/2009JE003351.

Roach, L. H., J. F. Mustard, S. L. Murchie, J.-P. Bibring, F. Forget, K. W. Lewis, O. Aharonson, M. Vincendon, and J. L. Bishop (2009), Testing evidence of recent hydration state change in sulfates on Mars, *J. Geophys. Res.*, *114*, E00D02, doi:10.1029/2008JE003245.

Ruff, S. W., and P. R. Christensen (2002), Bright and dark regions on Mars: Particle size and mineralogical characteristics based on Thermal Emission Spectrometer data, *J. Geophys. Res.*, *107*(E12), 5127, doi:10.1029/2001JE001580.

Savijärvi, H. (1995), Mars boundary layer modeling: Diurnal moisture cycle and soil properties at the Viking Lander 1 Site, *Icarus*, *117*, 120–127, doi:10.1006/icar.1995.1146.

Schröder, S., P.-Y. Meslin, A. Cousin, O. Gasnault, W. Rapin, J. Blank, J. Lasue, S. Maurice, R. C. Wiens, and MSL Science Team (2014), ChemCam hydrogen detection in soils and dust along Curiosity's traverse, in *8th International Conference on Mars*, p. 1214, Pasadena, Calif.

Sheather, S. J., and M. C. Jones (1991), A reliable data-based bandwidth selection method for kernel density estimation, *J. R. Stat. Soc. Ser. B*, *53*(3), 683–690.

Shimazaki, H., and S. Shinomoto (2010), Kernel bandwidth optimization in spike rate estimation, *J. Comput. Neurosci.*, *29*(1-2), 171–182, doi:10.1007/s10827-009-0180-4.

Steiger, M., K. Linnow, D. Ehrhardt, and M. Rohde (2011), Decomposition reactions of magnesium sulfate hydrates and phase equilibria in the $MgSO_4$-H_2O and Na^+-Mg^{2+}-Cl^--SO_4^{2-}-H_2O systems with implications for Mars, *Geochim. Cosmochim. Acta*, *75*(12), 3600–3626, doi:10.1016/j.gca.2011.03.038.

Vaniman, D. T., D. L. Bish, S. J. Chipera, C. I. Fialips, J. W. Carey, and W. C. Feldman (2004), Magnesium sulphate salts and the history of water on Mars, *Nature*, *431*(7009), 663–665, doi:10.1038/nature02973.

Wang, A., and Z. C. Ling (2011), Ferric sulfates on Mars: A combined mission data analysis of salty soils at Gusev crater and laboratory experimental investigations, *J. Geophys. Res.*, *116*, E00F17, doi:10.1029/2010JE003665.

Wang, A., J. J. Freeman, and B. L. Jolliff (2009), Phase transition pathways of the hydrates of magnesium sulfate in the temperature range 50°C to 5°C: Implication for sulfates on Mars, *J. Geophys. Res.*, *114*, E04010, doi:10.1029/2008JE003266.

Wang, A., W. C. Feldman, M. T. Mellon, and M. Zheng (2013), The preservation of subsurface sulfates with mid-to-high degree of hydration in equatorial regions on Mars, *Icarus*, *226*, 980–991, doi:10.1016/j.icarus.2013.07.020.

Wray, J. J., et al. (2011), Columbus crater and other possible groundwater-fed paleolakes of Terra Sirenum, Mars, *J. Geophys. Res.*, *116*, E01001, doi:10.1029/2010JE003694.

Yen, A. S., et al. (2008), Hydrothermal processes at Gusev Crater: An evaluation of Paso Robles class soils, *J. Geophys. Res.*, *113*, E06S10, doi:10.1029/2007JE002978.